CARRIER FREQUENCY AND DIRECTION OF ARRIVAL ESTIMATION WITH NESTED SUB-NYQUIST SENSOR ARRAY RECEIVER

A Anil Kumar, Sirajudeen Gulam Razul and Chong-Meng Samson See

Temasek Laboratories@NTU, 50 Nanyang Drive, Singapore 637553.
Email: {Anilkumar, eSirajudeen, SamsonSee}@ntu.edu.sg

ABSTRACT

Carrier frequency and its corresponding direction of arrival (DOA) estimation, at sub-Nyquist sampling rates of narrow-band (bandwidth not exceeding B Hz) sources is considered in this paper. We assume M physical sensors arranged in a two dimensional nested sensor array configuration and propose to modify the receiver architecture by inserting an additional delay channel to only the dense sensor array. An efficient subspace based estimation algorithm to estimate the carrier frequencies and their DOAs is also presented. With this proposed approach we show that a minimum ADC sampling frequency of B Hz is sufficient and $\mathcal{O}(\lceil M/4 \rceil^2)$ carrier frequencies and their DOAs can be estimated despite all the carrier frequencies exactly aliased to the same frequency. Furthermore, simulations indicate that when used for spectrum estimation, in addition to carrier frequencies and their DOA estimation, it shows better performance compared to an existing approach using the same M element uniform two dimensional sensor array.

Index Terms— Direction-of-arrival, sub-Nyquist sampling, Spectrum estimation, nested sensor array.

1. INTRODUCTION

In applications such as cognitive radios (CR), it is essential to have the knowledge of the occupied frequency band as well as their corresponding direction of arrival (DOA). These information will enable the CRs not only to utilize the unused spectrum but also would help in reducing the interference with the primary users [1]. The task of identifying the occupied spectrum bands can easily be accomplished by estimating their carrier frequencies. It is essential as well as important to estimate these parameters i.e., the carrier frequency and its corresponding DOA, at sub-Nyquist sampling rates. Estimating these quantities at sub-Nyquist sampling rate not only eliminates the necessity of high rate analog to digital converter (ADC), but also overcomes the subsequent high rate signal processing operations.

This problem of estimating the carrier frequencies and their DOAs at sub-Nyquist sampling rates have previously been addressed in [2] - [4]. [2] proposes to decompose the entire wide spectrum band into smaller bands, typically into 1GHz bands. Each decomposed smaller band is then split into direct path and delayed path, and subsequently samples the signal corresponding to each path at a sub-Nyquist sampling rate. Implementing this in practice is expensive, since this process of decomposing into smaller bands and then splitting into paths requires lot of hardware. On other hand, [3] proposes to employ a sub-Nyquist sampler such as multi-coset sampler [5] at the output of each sensor. In practice, a multi-coset sampler is realized through a multi-channel structure [6], and hence similar to the previous case even this approach requires more hardware. Recently, in [4] the authors of this paper, proposed a new approach, in which the receiver architecture is modified by introducing a single additional delayed branch at the output of every sensor. With this approach, it is shown that to estimate the complete signal spectrum blindly comprising of N narrow band unknown signals and their DOAs, $M \geq N + 1$ sensors are sufficient. Further it is also shown that an ADC sampling rate of atleast B Hz, where B denotes the maximum bandwidth of narrow-band signal, would suffice, thereby leading to a minimum overall sampling rate of $2MB = 2(N + 1)B$ Hz.

More recently, efficient DOA approaches which are based on certain sensor arrangements such as sparse ruler [7], nested ruler [8, 9] etc, have been proposed. These methods by using the second order statistics and intelligently exploiting the sensor arrangements show that more DOAs than the actual number of physical sensors can be identified. In particular, the nested array arrangement proposed in [8, 9] is attractive, since it is easy to construct for any M. In this paper, motivated by these recent developments, we propose to use the two dimensional nested array arrangement proposed in [9] by combining with the idea of modified receiver architecture described in [4], to increase the carrier frequency and their DOA estimation capacity. However, instead of trivially extending the idea of using the modified architecture by adding a delayed branch to the output of every sensor, here we propose to add the additional delayed branch only to those sensors placed at a denser scale in the nested array arrangement. With this modification, the algorithm proposed in [4] for the estimation of carrier frequencies and their DOAs cannot be directly employed. Hence, later in Section 3 we describe an alternative algorithm based on the idea of spatial smoothing, using which we can estimate upto $\lceil M/4 \rceil \geq \sqrt{N+1}$ (assuming equal number of sensors are allocated to sparse and dense array) carrier frequencies and their DOAs. Also, since the additional channel is only used for a subset of the physical sensors, unlike [4] the number of ADCs, thereby the minumum sampling rate of the system reduces; typically for a M sensor receiver, while with [4] it requires $2M$ ADCs and an overall minimum sampling rate of $2MB$ Hz, but with the proposed approach it requires only $(3M + 1)/2$ ADCs and an overall minimum sampling rate of

978-0-9928626-3-3/15/$31.00 ©2015 IEEE

$(3M+1)B/2$ Hz. Further, due to the increased degrees of freedom as a result of the nested arrangement, the spectrum estimation accuracy shows improvement when the proposed approach is used for spectrum estimation (assuming $N < M$) in addition to DOA and carrier frequency estimation. Later in Section 4, we shall demonstrate through simulations that the proposed approach shows better spectrum estimation performance compared to using the approach of [4] with the same M element two dimensional uniform sensor array.

2. PRELIMINARIES

In this section we first describe briefly the signal model and its frequency domain formulation provided in [4]. Then for the sake of completeness, a brief overview of the two dimensional nested arrays described in [9] is provided.

2.1. Signal model and frequency domain representation

N uncorrelated, disjoint, far field narrow-band signals with bandwidth not exceeding B Hz, which are spread within a very wide spectrum of $\mathcal{F} = [0, 1/T]$ is observed by a receiver consisting of M sensors. Such a signal which is commonly referred to as multi band signal (MBS) shall be denoted by $x(t)$ in time domain and can be expressed as

$$x(t) = \sum_{i=1}^{N} s_i(t) e^{j2\pi f_i t}. \tag{1}$$

Since the MBS $x(t)$ is bandlimited to the region $\mathcal{F}$, the Nyquist sampling rate of $x(t)$, $f_{nyq} = 1/T$. The signal observed by the l^{th} sensor, $l = \{1, 2, ..., M\}$ can be expressed as

$$x_l(t) = \sum_{i=1}^{N} s_i(t) e^{j2\pi f_i (t+\tau_l(\theta_i))} + \eta_l(t) \tag{2}$$

where $s_i(t)$, $i = \{1, 2, ..., N\}$ denotes the i^{th} source at baseband of bandwidth not exceeding B Hz with $B \ll 1/T$, $\{f_i\}_{i=1}^N$ denotes the N distinct *unknown* carrier frequencies and $\{\theta_i\}_{i=1}^N$ their corresponding DOA. The phase $\tau_l(\theta_i) = [\tau_l^x \quad \tau_l^y][\cos(\theta_i) \quad \sin(\theta_i)]^{\mathcal{T}}$, (τ_l^x, τ_l^y) denotes the l^{th} element of the sensor array given by the l^{th} position of the set S (refer (6)) and $[.]^{\mathcal{T}}$ denotes the transpose of the vector. The noise $\eta_l(t)$ is assumed to be white with variance σ_n^2 and uncorrelated with the sources.

The discrete time Fourier transform (DTFT) of the above signal obtained by sampling at a sub-Nyquist sampling rate of $f_s = 1/LT$ (i.e., the ADCs samples at every $t = nLT$),L denotes the sub-sampling factor, can be expressed in the following linear form as [4]

$$\mathbf{X}(f) = \underbrace{[\mathbf{a}(f_1, \theta_1), \ldots, \mathbf{a}(f_N, \theta_N)]}_{\mathbf{A}(\boldsymbol{f}, \boldsymbol{\theta})} \mathbf{S}(f) + \boldsymbol{\eta}(f) \tag{3}$$

where $\mathbf{X}(f) = [X_1(e^{j2\pi fT}), \ldots, X_M(e^{j2\pi fT})]^{\mathcal{T}}$, $X_l(e^{j2\pi fT})$ denotes the DTFT of $x_l(nLT)$, $\mathbf{S}(f) = [S_1^p(f), \ldots, S_N^p(f)]^{\mathcal{T}}$, $S_i^p(f)$ denotes the periodic aliased spectrum of i^{th} source signal, and for any $k \in \{1, 2, ...N\}$, the array manifold vector $\mathbf{a}(f_k, \theta_k) = [e^{j2\pi f_k \tau_1(\theta_k)}, \ldots, e^{j2\pi f_k \tau_M(\theta_k)}]^{\mathcal{T}}$. $\boldsymbol{f} = \{f_i\}_{i=1}^N$ and $\boldsymbol{\theta} = \{\theta_i\}_{i=1}^N$ denotes the unknown carrier frequency set and the DOA set respectively.

2.2. Nested arrays in two dimension

A brief introduction to two dimensional nested arrays is provided in this section. Interested readers may refer to [9] for more details on the construction of nested arrays in two dimension. Also, for the sake of simplicity in this paper we assume nested rectangular sensor array configuration, nevertheless the idea presented here can be extended to other classes which are outlined in [9]. A rectangular nested array is basically a concatenation of two uniform rectangular arrays (URAs): dense URAs with say M_d^x and M_d^y elements and a sparse URAs with say M_s^x and M_s^y elements along the two orthogonal axes respectively such that $M_s^x M_s^y + M_d^x M_d^y - 1 = M$. The sensor locations corresponding to the dense URA and sparse URA is given by

$$S_{dense} = \{(d/c)\mathbf{I}[p_x \quad p_y]^{\mathcal{T}}, 0 \le p_x < M_d^x, 0 \le p_y < M_d^y\} \tag{4}$$

$$S_{sparse} = \{(d/c)\mathbf{P}[p_x \quad p_y]^{\mathcal{T}}, 0 \le p_x < M_s^x, 0 \le p_y < M_s^y\} \tag{5}$$

where $\mathbf{I}$ denotes the identity matrix, $p_x, p_y \in \mathbb{Z}$, $d \le cT/2$ denotes the half wavelength spacing corresponding to the maximum frequency, which in this is $1/T$, and the matrix $\mathbf{P} = \begin{pmatrix} M_d^x & 0 \\ 0 & M_d^y \end{pmatrix}$. The sensor locations of the entire nested array is given by [9]

$$S = \{S_{dense} \cup S_{sparse}\}. \tag{6}$$

It may be observed that the array manifold matrix $\mathbf{A}(\boldsymbol{f}, \boldsymbol{\theta})$ resembles the two-dimensional (azimuth - elevation) DOA array manifold matrix [11]. However, the methods that are most often used in two-dimensional DOA estimation such as MUSIC algorithm which essentially searches along both the directions is not feasible in the present case. This is because not only the bandwidth of $x(t)$ is large (results in enormous search points), but it also results in ambiguity (refer to [10, Section IV]). Hence in [4], an additional delayed channel was added to every sensor using which the carrier frequencies could be easily determined. In the following section we propose a similar modification to the architecture by adding an additional channel, but unlike [4], we propose to add this additional channel only to the dense URA. This helps in further reducing the number of channels and thereby reduces the overall sampling rate.

3. PROPOSED APPROACH

We begin the description of the proposed approach by first describing the modifications to the receiver architecture and the corresponding formulations. We then describe an efficient reconstruction algorithm for estimation of carrier frequencies and their corresponding DOAs.

3.1. Modified receiver architecture and formulation

Fig. 1 shows the modified receiver architecture. It can be noticed that an additional delayed channel which delays the

signal by τT, $0 < \tau \leq 1$ is added only to the dense URA. Also, as shown in the figure, all the ADCs are synchronized and samples at a sub-Nyquist sampling rate of $f_s = 1/LT$ i.e., at every $t = nLT$. Compared to the existing approaches outlined in Section 1, the hardware requirement is minimized; typically it requires $2M_d + M_s$ ADCs, where $M_d = M_d^x M_d^y$ and $M_s = M_s^x M_s^y - 1$, denotes the number of dense and sparse URA sensors respectively.

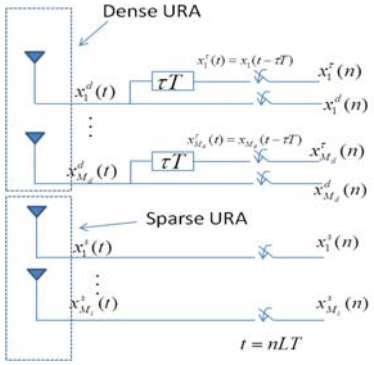

Fig. 1. Proposed multi-channel receiver architecture. The delayed branch which delays the signal by $\tau T, 0 < \tau \leq 1$ is added to only the dense URA.

Let $\{x_i^d(n)\}_{i=1}^{M_d}$, $\{x_i^s(n)\}_{i=1}^{M_s}$ and $\{x_i^\tau(n)\}_{i=1}^{M_d}$ denote the time domain samples corresponding to the direct path dense URA, direct path sparse URA and the additional delayed path dense URA respectively. Correspondingly, their DTFTs be denoted by $\{X_i^d(f)\}_{i=1}^{M_d}$, $\{X_i^s(f)\}_{i=1}^{M_s}$ and $\{X_i^\tau(f)\}_{i=1}^{M_d}$. Using (3), the combined DTFT vector $\mathbf{X}_{total}(f) = [\mathbf{X}_d(f), \mathbf{X}_s(f), \mathbf{X}_\tau(f)]^\mathcal{T}$, which is composed of both the direct path as well as the delayed path DTFT vectors can be expressed as

$$\mathbf{X}_{total}(f) = \underbrace{\begin{pmatrix} \mathbf{A}_d(\boldsymbol{f},\boldsymbol{\theta}) \\ \mathbf{A}_s(\boldsymbol{f},\boldsymbol{\theta}) \\ \mathbf{A}_\tau(\boldsymbol{f},\boldsymbol{\theta}) \end{pmatrix}}_{\mathbf{A}_{total}(\boldsymbol{f},\boldsymbol{\theta})} \mathbf{S}(f) + \mathbf{N}(f)$$

where $\mathbf{A}_d(\boldsymbol{f},\boldsymbol{\theta})$, $\mathbf{A}_s(\boldsymbol{f},\boldsymbol{\theta})$ and $\mathbf{A}_\tau(\boldsymbol{f},\boldsymbol{\theta})$ denotes the array manifold matrix corresponding to the direct path dense URA, direct path sparse URA and the delayed path dense URA respectively. The array manifold matrix for the delayed path $\mathbf{A}_\tau(\boldsymbol{f},\boldsymbol{\theta})$ can be expressed as [4], $\mathbf{A}_\tau(\boldsymbol{f},\boldsymbol{\theta}) = \mathbf{A}_d(\boldsymbol{f},\boldsymbol{\theta})\mathcal{D}$, where $\mathcal{D}$ is a diagonal matrix of order N with the diagonal elements $\{e^{-j2\pi f_1 \tau T}, e^{-j2\pi f_2 \tau T}, ..., e^{-j2\pi f_N \tau T}\}$. Now, using (7), we estimate the following covariance matrix

$$\begin{aligned} \mathbf{R}_{XX}^{total} &= \int_{f\in[0,f_s]} \mathbf{X}_{total}(f)\mathbf{X}_{total}^H(f)df \\ &= \mathbf{A}_{total}(\boldsymbol{f},\boldsymbol{\theta})\mathbf{R}_{ss}\mathbf{A}_{total}^H(\boldsymbol{f},\boldsymbol{\theta}) + \sigma_n^2\mathbf{I} \end{aligned} \quad (7)$$

where $\mathbf{R}_{ss} = \int_{f\in[0,f_s]} \mathbf{S}(f)\mathbf{S}^H(f)$ denotes the source covariance matrix. Due to the assumption of uncorrelated sources, $\mathbf{R}_{ss}$ can be assumed to be a diagonal matrix with diagonal elements $\mathbf{P} = [\sigma_{s_1}^2, \sigma_{s_2}^2 ... \sigma_{s_N}^2]^\mathcal{T}$, $\{\sigma_{s_k}^2\}_{k=1}^N$ denotes the signal power of the k^{th} source. Now, the vectorized $\mathbf{R}_{XX}^{total}$ can be expressed as

$$\mathbf{z} = \text{vec}(\mathbf{R}_{XX}^{total}) = \mathbf{A}_{total}^*(\boldsymbol{f},\boldsymbol{\theta}) \otimes \mathbf{A}_{total}(\boldsymbol{f},\boldsymbol{\theta})\text{vec}(\mathbf{R}_{ss}) + \sigma_n^2\mathbf{I}$$

$$= \begin{pmatrix} \mathbf{A}_d(\boldsymbol{f},\boldsymbol{\theta}) \\ \mathbf{A}_s(\boldsymbol{f},\boldsymbol{\theta}) \\ \mathbf{A}_\tau(\boldsymbol{f},\boldsymbol{\theta}) \end{pmatrix}^* \odot \begin{pmatrix} \mathbf{A}_d(\boldsymbol{f},\boldsymbol{\theta}) \\ \mathbf{A}_s(\boldsymbol{f},\boldsymbol{\theta}) \\ \mathbf{A}_\tau(\boldsymbol{f},\boldsymbol{\theta}) \end{pmatrix} \mathbf{P} + \sigma_n^2\mathbf{I} \quad (8)$$

where $'\otimes'$ and $'\odot'$ denotes the Kronecker product and Khatri-Rao product respectively, and $'*'$ denotes the conjugate operator. The above simplification from Kronecker product to Khatri-Rao product is due to the diagonal matrix structure of $\mathbf{R}_{ss}$. Let $\mathbf{z}_v$ and $\mathbf{z}_v^\tau$ denote a subset of the elements of $\mathbf{z}$ which are chosen as

$$\mathbf{z}_v = \mathbf{A}_v(\boldsymbol{f},\boldsymbol{\theta})\mathbf{P} + \sigma_n^2\mathbf{I} \quad (9)$$

$$\mathbf{z}_v^\tau = \mathbf{A}_v^\tau(\boldsymbol{f},\boldsymbol{\theta})\mathbf{P} + \sigma_n^2\mathbf{I} \quad (10)$$

where $\mathbf{A}_v(\boldsymbol{f},\boldsymbol{\theta}) = \mathbf{A}_d(\boldsymbol{f},\boldsymbol{\theta})^* \odot \mathbf{A}_s(\boldsymbol{f},\boldsymbol{\theta})$ and $\mathbf{A}_v^\tau(\boldsymbol{f},\boldsymbol{\theta}) = \mathbf{A}_\tau(\boldsymbol{f},\boldsymbol{\theta})^* \odot \mathbf{A}_s(\boldsymbol{f},\boldsymbol{\theta})$. If the nested array locations are chosen as described in Section 2.2, then it may easily be observed that the array manifold matrix $\mathbf{A}_v(\boldsymbol{f},\boldsymbol{\theta})$ corresponds to the direct path URA with locations given by

$$\begin{aligned} S_v = \{(d/c)\mathbf{I}[p_x \quad p_y]^\mathcal{T}, -M_d^x \leq p_x < M_d^x(M_s^x - 1), \\ -M_d^y \leq p_y < M_d^y(M_s^y - 1)\}. \end{aligned} \quad (11)$$

Similarly it can be observed that $\mathbf{A}_v^\tau(\boldsymbol{f},\boldsymbol{\theta})$ provides the delayed path array manifold matrix corresponding to the locations of S_v, and thus can be expressed as $\mathbf{A}_v^\tau(\boldsymbol{f},\boldsymbol{\theta}) = \mathbf{A}_v(\boldsymbol{f},\boldsymbol{\theta})\mathcal{D}$. This new URA whose locations are given by S_v is usually referred to as the *difference* URA [9].

P however is a single column vector and hence the estimation algorithm proposed in [4] cannot be directly applied here to estimate the carrier frequencies and their corresponding DOAs. Hence in the following section we outline a rank enhancing algorithm making use of $\mathbf{z}_v$ and $\mathbf{z}_v^\tau$ using which we can estimate both these quantities efficiently.

3.2. Estimation algorithm

The rank enhancing algorithm described in this section is based on the idea of two-dimensional spatial smoothing introduced in [10].

3.2.1. Formation of data matrices

Let M_v^x and M_v^y denote the lengths of the URA S_v, along the two orthogonal axes, which are essentially given by (see (11)) $M_v^x = M_s^x M_d^x$ and $M_v^y = M_s^y M_d^y$. Also, let $z_v(x,y)$ and $z_v^\tau(x,y)$ denote the data in the vector $\mathbf{z}_v$ and $\mathbf{z}_v^\tau$ respectively, corresponding to the sensor location (x,y). Let us define matrices $[\mathbf{B}_{m,n}]_{a,b} = z_v(a+m+\lceil M_v^x/2\rceil, b+n+\lceil M_v^y/2\rceil)$ and $[\mathbf{B}_{m,n}^\tau]_{a,b} = z_v^\tau(a+m+\lceil M_v^x/2\rceil, b+n+\lceil M_v^y/2\rceil)$, where $\{0 \leq a < m\}$, $\{0 \leq b < n\}$. The matrices $\mathbf{B}_{m,n}$ and $\mathbf{B}_{m,n}^\tau$ contains the data of the URA S_v corresponding to the locations $\{(x,y), m < x \leq m+\lceil M_v^x/2\rceil, n < y \leq n+\lceil M_v^y/2\rceil\}$. Now, we form the following data matrices

$$\begin{aligned} \mathbf{D} = [&\text{vec}(\mathbf{B}_{p_1,p_2}), ..., \text{vec}(\mathbf{B}_{p_1,p_2+\lceil M_v^x/2\rceil}), \text{vec}(\mathbf{B}_{p_1+1,p_2}), \\ &..., \text{vec}(\mathbf{B}_{p_1+1,p_2+\lceil M_v^x/2\rceil}), ..., \text{vec}(\mathbf{B}_{p_1+\lceil M_v^y/2\rceil,p_2+\lceil M_v^x/2\rceil})] \end{aligned} \quad (12)$$

$$\begin{aligned} \mathbf{D}^\tau = [&\text{vec}(\mathbf{B}_{p_1,p_2}^\tau), ..., \text{vec}(\mathbf{B}_{p_1,p_2+\lceil M_v^x/2\rceil}^\tau), \text{vec}(\mathbf{B}_{p_1+1,p_2}^\tau), \\ &..., \text{vec}(\mathbf{B}_{p_1+1,p_2+\lceil M_v^x/2\rceil}^\tau), ..., \text{vec}(\mathbf{B}_{p_1+\lceil M_v^y/2\rceil,p_2+\lceil M_v^x/2\rceil}^\tau)] \end{aligned} \quad (13)$$

where $p_1 = -M_d^y$, $p_2 = -M_d^x$. The above data matrices which are of size $\lceil M_v^x/2 \rceil \lceil M_v^y/2 \rceil \times \lceil M_v^x/2 \rceil \lceil M_v^y/2 \rceil$ can be decomposed as

$$\mathbf{D} = [\mathbf{a}_{left}(f_1, \theta_1) ... \mathbf{a}_{left}(f_N, \theta_N)] \mathbf{R}_{ss} \mathbf{A}_{new}^H(\boldsymbol{f}, \boldsymbol{\theta}) + \sigma_n^2 \mathbf{I} \quad (14)$$

$$\mathbf{D}^\tau = [\mathbf{a}_{left}(f_1, \theta_1) ... \mathbf{a}_{left}(f_N, \theta_N)] \mathbf{R}_{ss} \mathcal{D}^H \mathbf{A}_{new}^H(\boldsymbol{f}, \boldsymbol{\theta}) + \sigma_n^2 \mathbf{I} \quad (15)$$

where $\mathbf{a}_{left}(f_k, \theta_k)$ denotes the array manifold vector for the carrier frequency f_k and DOA θ_k, corresponding to the locations of vec($\mathbf{B}_{-M_d^y, -M_d^x}$) and the array manifold matrix $\mathbf{A}_{new}(\boldsymbol{f}, \boldsymbol{\theta}) = [\mathbf{a}_{new}(f_1, \theta_1) ... \mathbf{a}_{new}(f_N, \theta_N)]^H$, the array manifold vector $\mathbf{a}_{new}(f_k, \theta_k)$ is given by

$$\mathbf{a}_{new}(f_k, \theta_k) = [1, e^{j2\pi\omega_x^k}, ..., e^{j2\pi\lceil M_v^x/2 \rceil \omega_x^k}, e^{j2\pi(\omega_x^k + \omega_y^k)}, \\ ... e^{j2\pi(\lceil M_v^x/2 \rceil \omega_x^k + \omega_y^k)} ... e^{j2\pi(\lceil M_v^x/2 \rceil \omega_x^k + \lceil M_v^y/2 \rceil \omega_y^k)}]^H \quad (16)$$

where $\omega_x^k = (d/c) f_k \cos(\theta_k)$ and $\omega_y^k = (d/c) f_k \sin(\theta_k)$.

3.2.2. Estimation of carrier frequencies and DOA

Using the above data matrices $\mathbf{D}$ and $\mathbf{D}^\tau$, we form the following covariance matrices

$$\mathbf{R}_{DD} = \mathbf{D}^H \mathbf{D} \quad (17)$$

$$\mathbf{R}_{D^\tau D} = (\mathbf{D}^\tau)^H \mathbf{D}. \quad (18)$$

Assuming $N < \lceil M_v^x/2 \rceil \lceil M_v^y/2 \rceil$, similar to [4] under no-noise condition it can easily be shown that the N generalized eigenvalues (GEs), say $\{\lambda_i\}_{i=1}^N$, of the matrix pencil $\{\mathbf{R}_{D^\tau D}, \mathbf{R}_{DD}\}$, would yield the diagonal values of $\mathcal{D}^*$. By using these GE's the carrier frequencies can then be estimated using

$$\hat{f}_i = \frac{\arg \lambda_i}{2\pi\tau T} \quad , i = \{1, 2, ..., N\}. \quad (19)$$

While under no-noise condition, the above equation would yield exact carrier frequencies, however under the presence of noise the GE's are perturbed, and hence the estimated carrier frequencies shall be deviated from the true values. Also since $0 < \tau \leq 1$, it can easily be noticed from the above equation that the frequency errors gets amplified by $1/\tau$, and hence in practice it is always preferable to choose τ closer to 1.

Upon estimation of the carrier frequencies, the signal subspace and noise subspace of $\mathbf{R}_{DD}$ can be estimated by using the eigenvalue decomposition. Now, using $\mathbf{a}_{new}(f_k, \theta_k)$ as the signal space spanning vectors, MUSIC algorithm can then be employed to estimate DOA θ_k corresponding to the carrier frequency $f_k, \forall k = \{1, 2, ..., N\}$. To further improve the accuracy of the estimated carrier frequency and also to estimate DOA in a computationally efficient manner, the computationally efficient two-dimensional multi-resolution algorithm described in [4] can be employed.

If in addition to carrier frequencies and DOAs, signal spectrum is required then by assuming $N \leq M$, the array manifold matrix $\mathbf{A}(\boldsymbol{f}, \boldsymbol{\theta})$ can be formed with the estimated frequency and DOA, and by using (3) $\mathbf{S}(f)$ can be estimated. The signal spectrum can then be estimated by following the method outlined in [4, Section 3.3.2].

3.3. Minimum sampling rate

Proposition 3.1 *With the two-dimensional nested array arrangement outlined in Section 2.2 and further assuming sources are uncorrelated, the N carrier frequencies and their DOAs are completely recoverable (assuming no-noise) using the proposed approach if*
i) $N < \lceil M_v^x/2 \rceil \lceil M_v^y/2 \rceil$
ii) $L \leq 1/BT$ *(i.e.,* $f_s \geq B$*).*

As shown in [9], to obtain maximum gain from nesting, almost same number of elements must be allocated to both the sparse and dense URAs. Assuming that $(M+1)/2$ sensors are allocated to each of the dense as well as the sparse URA, it can easily be observed from the above proposition that upto $\lceil M/4 \rceil^2 - 1$ carrier frequencies and their DOAs can be estimated. Now, by taking the lower limit on the second condition, and with the above sensor arrangement assumption, the overall minimal sampling rate of the entire proposed receiver would be $f_{min}^{prop} = (3M+1)B/2$. Since $B \ll 1/T$, $f_{min}^{prop} \ll f_{nyq}$.

4. SIMULATION RESULTS

In this section, we present the simulation results to illustrate the capability and performance of the proposed approach. For all our simulations, we fix $\mathcal{F} = [0, 5]$ GHz and $B = 10$ MHz. A nested array with dense URA of $M_d^x = M_d^y = 3$ sensors and a sparse URA with the same number of elements are chosen. This corresponds to a total of $M = 17$ physical sensors (see Section 2.2). The locations of the dense and the sparse URAs are generated according to (4) and (5) respectively. This configuration provides a difference URA with $M_v^x = M_v^y = 9$.

First we conducted simulation to test the maximum frequency and DOA estimation capacity with the proposed approach. With the above nested configuration, as shown by Proposition 3.1, upto $\lceil M_v^x/2 \rceil \lceil M_v^y/2 \rceil - 1 = 24$ carrier frequencies and their DOAs can be estimated and hence we choose $N = 24$ for this simulation. Also, we fix the sampling frequency of ADC to $f_s = 10$ MHz (corresponding to the lower limit of the second condition described by Proposition 3.1). Observe that since $f_s = B = 10$ MHz, all the 24 information bands will completely alias between [0,10] MHz. Fig. 2 shows the scatter plot of the actual and estimated carrier frequencies and their corresponding DOAs. From the plot it may be observed that all 24 carrier frequencies and their DOAs are properly estimated despite all the bands being completely aliased and $N > M$.

Next, we performed simulations to compare the spectrum estimation performance with the proposed approach. The performance is compared against the approach of [4] with a URA of size 6×3 and also with an oracle method of the same URA dimension. In the oracle method, the signal is reconstructed by assuming the carrier frequencies and their DOAs are perfectly known. The URA dimension of 6×3 is chosen since it requires approximately the same number of physical sensors required by the nested array configuration chosen here. For this simulation, we fix $N = 10$ sources with carrier frequencies $\boldsymbol{f} = \{300, 550, 800, 1050, 1300, 1800, 2050, 2300,$

$2800, 3550\}$ MHz and their corresponding DOAs $\boldsymbol{\theta} = \{100, 130, 50, 150, 30, 200, 235, 250, 310, 350\}$ deg. Further we fix the ADC sampling frequency to $f_s = 250$ MHz. With this sampling frequency and the choice of the carrier frequencies, it may be noticed that all the bands exactly alias around 50 MHz following the sub-Nyquist sampling. Fig. 3 shows the RMSE performance plots for the nested array (proposed approach), the approach of [4] with the URA 6×3 and the oracle method. From the figure it may be noticed that the proposed approach performs better and approaches closer to the performance of the oracle method faster when compared to the URA with 6×3 elements. The covariance matrix dimension for this nested configuration with the proposed approach is 25×25, while for the 6×3 URA elements with the approach of [4] it is 18×18. Because of this increased matrix dimension, the nested array based approach proposed here seems to perform better compared to 6×3 URA.

It is also important to notice the reduction in the hardware and the sampling frequency with the proposed approach; while the proposed scheme requires only 26 ADCs (overall sampling frequency = 6.5 GHz), but estimating with the regular 6×3 URA (using the approach of [4]) requires 36 ADCs (overall sampling frequency = 9 GHz).

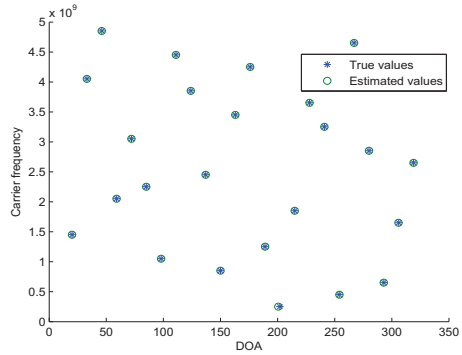

Fig. 2. Scatter plot of carrier frequency and their corresponding DOA for 24 sources

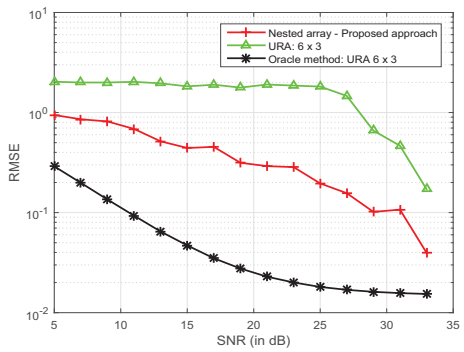

Fig. 3. RMSE vs SNR performance comparison of the estimated spectrum.

5. CONCLUSION

The problem of estimation of carrier frequencies and their corresponding DOAs of N narrow band signals spread within a large spectrum band, sampled at sub-Nyquist sampling rate is considered in this paper. We assume a two-dimensional nested array arrangement of M physical sensors and a modification to the architecture by adding an additional delayed branch to only the dense sensor array is proposed. An efficient estimation algorithm based on the second order statistics is also presented in this paper. With this proposed approach, we showed that for a two dimensional nested array comprising of M physical sensor elements, upto $\lceil M/4 \rceil^2 - 1$ carrier frequencies and their DOAs can be estimated even when all the frequencies exactly alias to the same frequency. Further, through simulations we demonstrated that the proposed approach when used for spectrum estimation in addition to carrier frequency and DOA estimation, shows improved RMSE performance compared to the same M element, uniform two dimensional array.

6. REFERENCES

[1] J. Werner, J. Wang, A. Hakkarainen, and M. Valkama, "Primary user localization in cognitive radio networks using sectorized antennas," in *2013 10th Annual Conf. on Wireless On-demand Network Systems and Services (WONS),* Banff, Canada, Mar. 2013.

[2] M. D. Zoltowski and C. O. Mathews, "Real-time frequency and 2-D angle estimation with sub-Nyquist spatio-temporal sampling," *IEEE Trans. on Signal Process.,* Vol. 42, PP. 2781-2794, Oct. 1994.

[3] D. D. Ariananda and G. Leus, "Compressive joint angular-frequency power spectrum estimation," in *Proc. European Signal Processing conference 2013 (EUSIPCO' 2013)*, Sep. 2013

[4] A. A. Kumar, S. G. Razul and C. M. S. See, "An efficient sub-Nyquist receiver architecture for spectrum blind reconstruction and direction of arrival estimation," in *Proc. IEEE Int. Conf. on Acous. Speech and Signal Process. 2014 (ICASSP' 2014)*, May 4-9, 2014.

[5] P. Feng and Y. Bresler, "Spectrum-blind minimum-rate sampling and reconstruction of multiband signals," in *Proc. IEEE Int. Conf. Acoust., Speech, Signal Process. (ICASSP) 1996*, Vol. 3, PP. 1688-1691, May 1996.

[6] M. Mishali and Y. C. Eldar, "Blind multiband signal reconstruction:compressed sensing for analog signals," *IEEE Trans. on Signal Process.*, Vol. 57, PP. 993-1009, Mar. 2009.

[7] S. Shakeri, D. D. Ariananda, and G. Leus, "Direction of arrival estimation using sparse ruler array design," *Proc. IEEE workshop on Signal Process. Adv. wireless commun.,* Cesme, Turkey, June 2012.

[8] P. Pal and P. P. Vaidyanathan, "Nested arrays: a novel approach to array processing with enhanced degrees of freedom," *IEEE Trans. on Signal Process.*, Vol. 58, PP. 4167-4181, Aug. 2010.

[9] P. Pal and P. P. Vaidyanathan, "Nested arrays in two dimensions, Part I: geometrical considerations," *IEEE Trans. on Signal Process.*, Vol. 60, PP. 4694-4705, Sep. 2012.

[10] P. Pal and P. P. Vaidyanathan, "Nested arrays in two dimensions, Part II: application in two dimensional array processing," *IEEE Trans. on Signal Process.*, Vol. 60, PP. 4706-4718, Sep. 2012.

[11] L. C. Godara, "Application of antenna arrays to mobile communications, part II: Beam-forming and direction-of-arrival considerations," *Proc. of the IEEE*, Vol. 85, PP. 1195-1245, Aug. 1997.